Expedite your small-field dosimetry workflow.

SRS MapCHECK™

SRS PATIENT QA, NO FILM

See it firsthand at AAPM 2018

Learn More

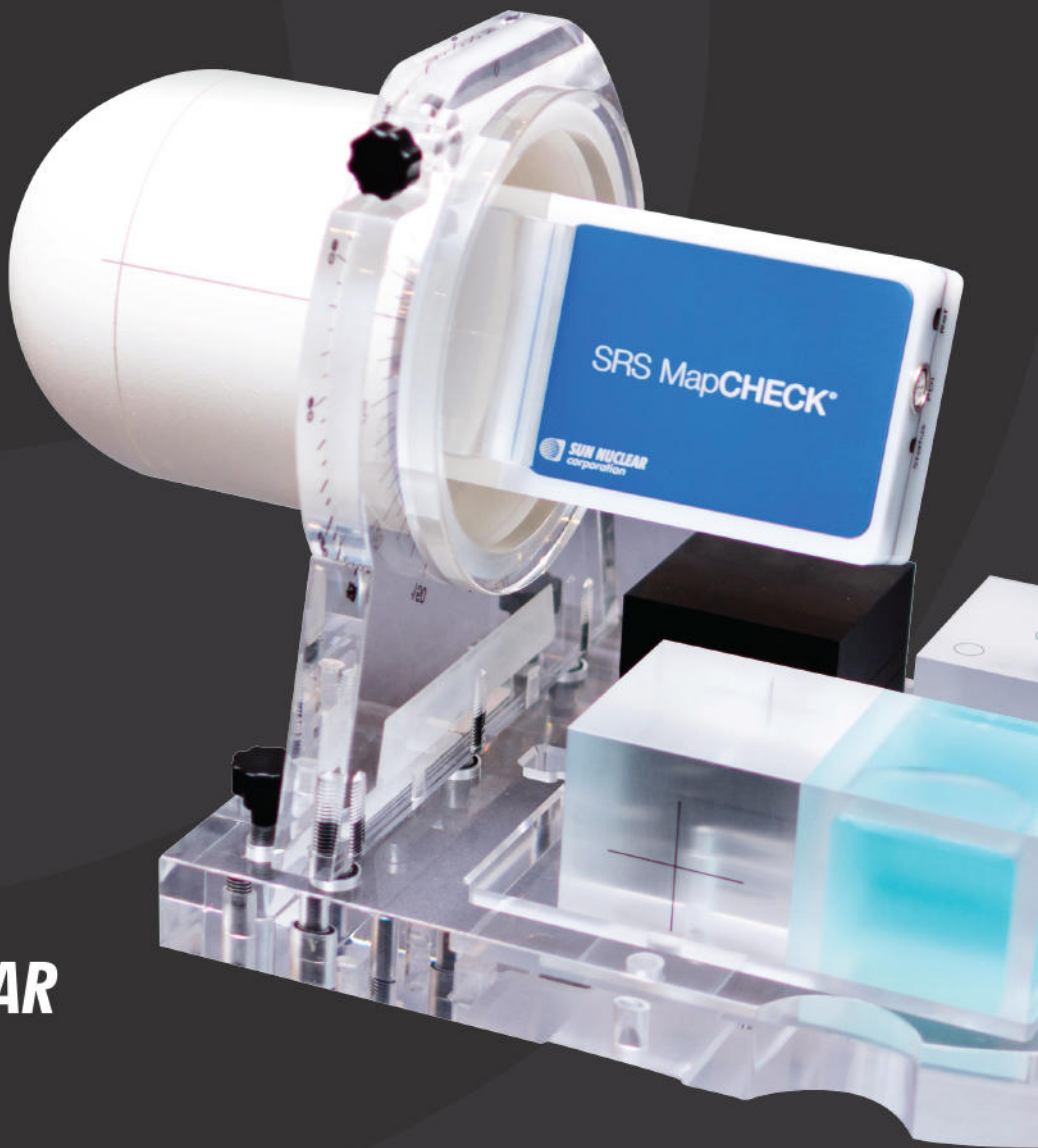

SUN NUCLEAR corporation

Image quality of conventional images of dual-layer SPECTRAL CT: A phantom study

Fasco van Ommen[a)] and Edwin Bennink
Radiology and Nuclear Medicine, UMC Utrecht, P.O. Box 85500, 3508 GA, Utrecht, The Netherlands
Image Sciences Institute UMC Utrecht, P.O. Box 85500, 3508 GA, Utrecht, The Netherlands

Alain Vlassenbroek
CT Clinical Science, Philips Healthcare, Brussels, Belgium

Jan Willem Dankbaar and Arnold M.R. Schilham
Radiology and Nuclear Medicine, UMC Utrecht, P.O. Box 85500, 3508 GA, Utrecht, The Netherlands

Max A. Viergever
Image Sciences Institute UMC Utrecht, P.O. Box 85500, 3508 GA, Utrecht, The Netherlands

Hugo W.A.M. de Jong
Radiology and Nuclear Medicine, UMC Utrecht, P.O. Box 85500, 3508 GA, Utrecht, The Netherlands
Image Sciences Institute UMC Utrecht, P.O. Box 85500, 3508 GA, Utrecht, The Netherlands

(Received 17 November 2017; revised 16 April 2018; accepted for publication 26 April 2018; published 28 May 2018)

Purpose: Spectral CT using a dual layer detector offers the possibility of retrospectively introducing spectral information to conventional CT images. In theory, the dual-layer technology should not come with a dose or image quality penalty for conventional images. In this study, we evaluate the influence of a dual-layer detector (IQon Spectral CT, Philips Healthcare) on the image quality of conventional CT images, by comparing these images with those of a conventional but otherwise technically comparable single-layer CT scanner (Brilliance iCT, Philips Healthcare), by means of phantom experiments.

Methods: For both CT scanners, conventional CT images were acquired using four adult scanning protocols: (a) body helical, (b) body axial, (c) head helical, and (d) head axial. A CATPHAN 600 phantom was scanned to conduct an assessment of image quality metrics at equivalent (CTDI) dose levels. Noise was characterized by means of noise power spectra (NPS) and standard deviation (SD) of a uniform region, and spatial resolution was evaluated with modulation transfer functions (MTF) of a tungsten wire. In addition, contrast-to-noise ratio (CNR), image uniformity, CT number linearity, slice thickness, slice spacing, and spatial linearity were measured and evaluated. Additional measurements of CNR, resolution and noise were performed in two larger phantoms.

Results: The resolution levels at 50%, 10%, and 5% MTF of the iCT and IQon showed small, but significant differences up to 0.25 lp/cm for body scans, and up to 0.2 lp/cm for head scans in favor of the IQon. The iCT and IQon showed perfect CT linearity for body scans, but for head scans both scanners showed an underestimation of the CT numbers of materials with a high opacity. Slice thickness was slightly overestimated for both scanners. Slice spacing was comparable and reconstructed correctly. In addition, spatial linearity was excellent for both scanners, with a maximum error of 0.11 mm. CNR was higher on the IQon compared to the iCT for both normal and larger phantoms with differences up to 0.51. Spatial resolution did not change with phantom size, but noise levels increased significantly. For head scans, IQon had a noise level that was significantly lower than the iCT, on the other hand IQon showed noise levels significantly higher than the iCT for body scans. Still, these differences were well within the specified range of performance of iCT scanners.

Conclusions: At equivalent dose levels, this study showed similar quality of conventional images acquired on iCT and IQon for medium-sized phantoms and slightly degraded image quality for (very) large phantoms at lower tube voltages on the IQon. Accordingly, it may be concluded that the introduction of a dual-layer detector neither compromises image quality of conventional images nor increases radiation dose for normal-sized patients, and slightly degrades dose efficiency for large patients at 120 kVp and lower tube voltages. *© 2018 The Authors. Medical Physics published by Wiley Periodicals, Inc. on behalf of American Association of Physicists in Medicine.* [https://doi.org/10.1002/mp.12959]

Key words: conventional images, dual-energy CT, dual-layer detector, image-quality, Spectral CT

1. INTRODUCTION

Dual-energy CT (DECT) has been an active research area since first investigated by Alvarez and Macovski in 1976.[1,2] However, owing to a number of technical difficulties DECT was not clinically applicable until recent advances in CT technology, and has since led to the introduction of several DECT systems. In DECT imaging two datasets are acquired at different energies. In this way DECT utilizes the property that materials have different attenuation coefficients at different energies, which allows for the differentiation of materials according to their attenuation characteristics.[3]

A number of dedicated dual-energy techniques have been commercially introduced over the past few years. These include scanners with (a) tube potential (kV) switching, (b) dual X-ray sources, (c) split X-ray beam, or (d) a dual-layer detector. The first three types only allow for prospective dual-energy DECT, in which the choice of acquisition, i.e. conventional imaging or dual-energy imaging, has to be made in advance. The fourth type has a dedicated dual-layer detector which allows retrospective DECT imaging. In tube potential switching scanners, such as the Discovery CT750 (GE Healthcare, Chicago, IL, USA), and dual X-ray source scanners, such as the Somatom Force (Siemens Healthcare, Erlangen, Germany), a specific DECT protocol has to be selected before the start of the acquisitions. This on the one hand provides a low- and high-energy dataset, but on the other hand has its limitations with respect to conventional imaging. The main limitation for kV switching is that both energy scans are limited to the same filtration, and therefore have a relatively high overlap of the energy spectra, and for dual X-ray sources the main limitations are a reduced field-of-view and cross scattering.[3,4] These limitations may be acceptable, because the benefits of DECT imaging may outweigh the limitations in certain diagnostic examinations.

Dual-layer detector CT scanners, such as the IQon Spectral CT (Philips Healthcare, Best, the Netherlands), always acquire two datasets, independent of protocol.[5] In the IQon Spectral CT, a single X-ray source is used to expose a detector, consisting of two scintillator layers. The top layer is more sensitive to the low-energy photons, whereas the bottom detector layer absorbs more of the high-energy photons. This essentially separates a single X-ray beam into two components.[4] The use of a dual-layer detector enables retrospective dual-energy analysis on every recorded dataset acquired at high tube voltage (e.g. 120 and 140 kVp). However, since in current clinical practice the dual-layer spectral CT scanner is mainly used for routine nonspectral imaging, these images should not come with a dose or image quality penalty compared to conventional CT images. The dual-layer technology allows the creation of conventional images, by virtue of the spatial and temporal alignment of the datasets from the two detector layers. This alignment allows adding up the sinograms from both layers for reconstruction of a conventional CT image, so that the detector essentially functions as a single-layer detector. In theory, this means that the data collected from the two layers is equivalent to the data collected with a single-layer detector, and thus hardly introduces any penalty regarding image quality. However, there are a number of substantial differences between the two detectors, which make this assumption not straightforward. An important factor is that the dual-layer detector has two electronic channels per detector element. Each read-out contributes electronical noise, resulting in increased higher electronical noise per detector element than in a single-layer detector with only one read-out. The electronic channels on the IQon, however, have an improved low-dose performance compared with the older electronic channels, which reduces noise slightly per channel as compared with the single-layer detector. In addition, the dual-layer detector has a higher X-ray stopping power, and a higher light output of the scintillators than the single-layer detector. Furthermore, the IQon has a tungsten backbone. The backbone does not only provide stability, but also reduces cross-talk. Lastly, the dual-layer detector has a slightly lower geometrical efficiency than a single-layer detector due to side read out. These differences all can influence image quality and dose efficiency, and raise the question to whether or not the dual-layer detector would perform similarly to a single-layer detector. The purpose of this study is to investigate the assumption that the acquisition on a dual-layer detector CT scanner does not influence dose efficiency and image quality of conventional images.

In an effort to determine the influence of the dual-layer detector, a performance characterization of the IQon was conducted at our institute and compared with the performance of a technically equivalent conventional single-layer CT scanner (Brilliance iCT, Philips Healthcare), using phantoms. The iCT was selected for this comparison, because the IQon and iCT are equal in terms of gantry and X-ray tube, except for a reduced titanium filtration in the IQon compared to the iCT to increase spectral separation between the low and high energies (i.e., increase the number of low energy photons).

2. MATERIALS AND METHODS

2.A. Scanning modes

To study the performance of the Philips IQon Spectral CT, a quantitative comparison with the Philips Brilliance iCT was made by comparing image quality of conventional images acquired on both scanners. The iCT was selected, because the hardware of the IQon and iCT scanners is equal (apart from the detector and tube filtration). Four regular adult scanning protocols were scanned on both the IQon and iCT: (a) body helical, (b) body axial, (c) head helical, and (d) head axial. These protocols were selected because these are used most at our institute, and because the wedge filter used on the iCT in these protocols matches the wedge filter of the IQon. Each protocol was scanned with tube voltages of 80, 100, 120, and 140 kVp, and with a fixed exposure of 200 mAs for the IQon. Other scan parameters are summarized in Table I. In order to reduce the likelihood of errors, all acquisitions were performed five times successively.

TABLE I. IQon and iCT scan parameters before dose matching for all scan types.

Scan type	Tube voltage (kVp)	Exposure (mAs)	Beam Collimation (Total collimation width) (mm)	Rotation time (s)	Scan arc (°)	Pitch (Body/Head)	Focal spot size (mm)	Views per gantry rotation (#)
Body/head Helical	80/100/120/140	200	64 × 0.625 (40)	0.33	NA	1.171/0.296	1.1 × 1.2	2400
Body/head Axial	80/100/120/140	200	64 × 0.625 (40)	0.33	360	NA	1.1 × 1.2	2400

2.B. Dose

There is a slight difference between the iCT and IQon with regard to tube filtration. To create a larger flux for the spectral separation on the IQon, the scanner has a reduced titanium filtration. To quantify the change in spectrum resulting from the reduced filtration, the half-value layer (HVL) was measured at all tube voltages on both the iCT and the IQon. In order to compensate for this difference in flux, the exposure values (mAs) of the iCT were selected such that the dose of the scanning protocols on the iCT matched the dose of the scanning protocols of the IQon. The volume CT dose index (CTDI) was measured for the body and head scans using a body and head phantom (IBA Dosimetry, Bartlett, TN, USA), respectively, each with a 10 cm pencil ionization chamber (Raysafe, Billdal, Sweden). First, the iCT scan parameters were set equal to the scan parameters used on the IQon. When the difference between the CTDIs was too large, the exposure value of the protocol on the iCT was changed to match the dose of the IQon. A difference in CTDI up to 5% was accepted, corresponding to an uncertainty in exposure up to 10 mAs.

2.C. Image reconstruction

Images were reconstructed using the default hybrid iterative reconstruction method iDose[4] (level: 1), with standard reconstruction filter for body and head ("B" and "UB", respectively) for both the iCT and the IQon. The iDose[4] (level: 1) reconstruction was chosen because it was available on both machines and it keeps the amount of postprocessing minimal. Images were reconstructed to 1 mm slice thickness and 1 mm slice spacing, using a field-of-view (FOV) of 250 mm and a reconstruction matrix of 512 × 512 pixels.

2.D. Image quality

To study the image quality of both CT scanners, a phantom study was conducted using a Catphan 600 phantom containing five modules (The Phantom Laboratory, Salem, NY, USA). The phantom was positioned in the isocenter of the scanner as suggested by the user manual.[6]

Catphan module CTP404 was used to measure *CT number linearity*, *spatial linearity*, *slice thickness,* and *slice spacing*. This module contains seven inserts with different opacity, which have a range of approximately −1000 to 1000 Hounsfield units (HUs). Spatial linearity is verified by measuring the distances between three 3 mm holes with a fixed distance (50 mm). Slice thickness and slice spacing can be estimated using two sets of 23° wire ramps, by measuring the full width at half maximum length and multiplying this with a 23° ramp angle correcting factor as instructed by the user manual.[6]

Module CTP591 was used to measure *spatial resolution* via the modulation transfer function (MTF). The MTF was calculated using a 50 μm tungsten wire source. This wire source is used to calculate a point spread function (PSF), from which the MTF was computed using a Fourier transform, and normalized to the average intensity of the PSF:[7]

$$MTF\ (f_x) = \frac{|DFT[I(x)]|}{I}.$$

For every acquisition, an MTF was calculated from the x-direction PSF and y-direction PSF. The wire source has a finite size, whereas an MTF is calculated from an infinitesimal point source. To correct for the finite size of the wire source, the following correction factor is used:[8]

$$CF(u) = 2\frac{J_1(\pi ud)}{\pi ud},$$

in which J_1 is the first order Bessel function, u the spatial frequency and d the diameter of the wire source. To compare the two scanners, the resolutions corresponding to 50%, 10%, and 5% MTF were calculated. In addition, module CTP528 was used to visually verify the spatial resolution.

Module CTP515 was used to calculate the *contrast-to-noise ratio* (CNR) of a 1.0% nominal contrast target with a 15 mm diameter. A region of interest (ROI) was selected in the target, and a region of the same size was selected in the background. CNR was then calculated as:

$$CNR = \frac{\overline{I}_{ROI} - \overline{I}_{bg}}{\sqrt{\frac{1}{2}(\sigma_{ROI}{}^2 + \sigma_{bg}{}^2)}}.$$

Here, $\overline{I}_{ROI}$ is the average signal of the ROI, $\overline{I}_{bg}$ the average signal of the background, σ_{ROI} the standard deviation of the ROI and σ_{bg} the standard deviation of the background. CNR was calculated in five consecutive slices in every acquisition, and from these five acquisitions an average CNR was calculated.

Module CTP486 is cast from a uniform material, of which the CT number (expected range: 5–18 HU) is designed to be within 2% of that of water. The module was used to measure the accuracy of the system by calculating a *mean CT number*, and to *characterize noise* by calculating the standard deviation (SD) of the mean CT number and by measuring the noise power spectrum (NPS). Nine ROIs of 64 × 64 voxels were

selected in the uniform material, of which the SD was calculated and the 2D NPS was computed using the discrete Fourier transform:[7]

$$NPS(f_x,f_y) = \frac{1}{R}\sum_{i=1}^{R}\left|DFT_{2D}\left[I_i(x,y)-\bar{I}_i\right]\right|^2\frac{\Delta_x\Delta_y}{N_xN_y}.$$

Here, $I_i(x,y)$ is the signal in the i-th ROI, $\bar{I}_i$ the mean of $I_i(x,y)$ and R the total number of ROIs. The quantities Δ_x, Δ_y, N_x and N_y are the pixel spacing and the number of pixels in the x- and y-directions. With radial averaging, the 2D NPS can be collapsed to a 1D radial frequency.[7] The mean CT number was calculated for each acquisition by calculating the mean HU value of the nine ROIs.

To study the effects of beam hardening due to patient size in body scans, an analysis of the Catphan phantom with additional attenuation was conducted. Around the Catphan phantom infusion bags filled with water were positioned, widening the diameter of the Catphan from 20 to 34 cm. The same setup was scanned on both the iCT and IQon. From these images the SD, NPS, MTF, and CNR were calculated. In addition, to study the effect of very large patients in body scans, the body phantom was surrounded with water infusion bags, to create a phantom of 45 cm in diameter. Since such large phantoms require more penetrating radiation, they were scanned at 120 and 140 kVp on both the iCT and IQon. From these images the SD and NPS was calculated.

2.E. Statistical analysis

All measurements were repeated five times to allow testing for statistical significance between the average values of the two scanners, by using an unpaired-sample t test. A significance level of 0.05 was chosen. For the comparison of the NPS, to account for multiple sampling, a Bonferroni correction was applied. The null hypothesis is that IQon and iCT show equal performance at equivalent dose.

3. RESULTS

3.A. Dose

The HVL measurements of the iCT showed an increase in HVL compared to the IQon (Table II).

For both body and head scans, the dose measurements showed a more than 5% lower dose on the iCT than on the IQon, as can be seen in Table III. Accordingly, to compensate for the dose difference, body scans on the iCT at 80, 100, 120 and 140 kVp were acquired with an exposure value of 250, 240, 240, and 230 mAs respectively. Similarly, head scans on the iCT at 80, 100, 120, and 140 kVp were acquired with an exposure value of 250, 240, 230, and 220 mAs. Furthermore, the CTDI values as reported by the scanner are comparable to the measured CTDIs (Table III).

TABLE II. Half-value layer measurements (mm Al) at different tube voltages.

	Body scans		Head scans	
	IQon	iCT	IQon	iCT
80 kVp	5.19	6.47	5.05	6.56
100 kVp	6.86	8.27	6.88	8.36
120 kVp	7.97	9.59	8.13	9.65
140 kVp	9.27	10.8	9.12	10.7

3.A.1. CT number linearity

For both scanners, the body scans showed unbiased CT-number linearity. HU values in those scans were in accordance with expected values as stated in the user manual of the phantom [Fig. 1(a)]. The head scans, however, showed significantly underestimated HU values for the high opacity inserts (Delrin: expected 344–387 HU and Teflon: expected 941–1060 HU). The underestimation was visible at all energies for the IQon, and for the iCT at 100, 120, and 140 kVp. For the iCT at 80 kVp only the Teflon insert was outside the range of expected values [Fig. 1(b)]. Figure 1 is exemplary for axial scans.

3.A.2. Spatial linearity, slice thickness, and slice spacing

The mean distances measured to evaluate spatial linearity were all found to be within 0.1 mm of the expected value of 50 mm. The differences between the iCT and IQon were not significant.

For both scanners, slice spacing was in accordance with the set reconstruction parameter of 1 mm, and there is no significant difference between the scanners.

In general, the slice thickness was overestimated by both scanners, with every scan type (Table IV). There were no significant differences in head scans between the two scanners. For body scans, however, there was a significant difference at the 140 kVp measurements. In addition, the body axial scans at 100 and 120 kVp showed a significant difference.

3.A.3. Spatial resolution

MTF curves, presented in Fig. 2, showed a similar shape for all scan protocols on both scanners at all energies. However, the MTF curves of the iCT appeared to vary slightly with tube voltage, whereas those of the IQon were less dependent on tube voltage.

The corresponding 50%, 10%, and 5% MTF curves showed differences in resolution between IQon and iCT up to 0.25 line pairs per cm (lp/cm) for body scans as shown in Table V and differences up to 0.2 lp/cm for head scans, as shown in Table VI. The resolving power of body scans acquired on the IQon is generally slightly higher than on the iCT, but this difference is not always significant. Overall, the resolution of body scans was slightly higher than that of head scans.

TABLE III. CTDI measurements (mGy) at different tube voltages before dose matching. The CTDIs reported in the protocol are stated between brackets.

	Body scans			Head scans		
	IQon	iCT	Difference (%)	IQon	iCT	Difference (%)
80 kVp	6.13 (6.00)	4.54 (4.20)	25.93	11.85 (11.9)	9.00 (8.70)	24.04
100 kVp	11.87 (11.4)	9.45 (8.80)	20.34	22.32 (22.2)	17.68 (17.5)	20.78
120 kVp	18.81 (18.1)	15.18 (14.7)	19.31	34.16 (34.3)	29.18 (28.7)	14.58
140 kVp	25.91 (26.0)	22.00 (21.6)	15.09	48.35 (48.6)	43.15 (41.9)	10.76

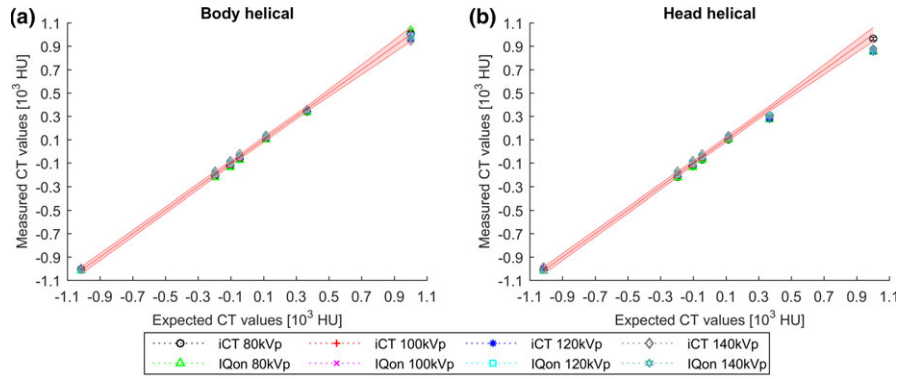

FIG. 1. Comparison of CT values (HU) at all energies of IQon and iCT of (a) body helical scans and (b) head helical scans. The range of expected values is indicated by the shaded area. [Color figure can be viewed at wileyonlinelibrary.com]

TABLE IV. Comparison of reconstructed slice thickness (mean ± SD) (mm) for all scan types and energies. If the difference between IQon and iCT values is significant, both values are marked with an asterisk.

	80 kVp	100 kVp	120 kVp	140 kVp
Body helical				
IQon	1.27 ± 0.09	1.19 ± 0.17	1.27 ± 0.09	1.39 ± 0.09*
iCT	1.19 ± 0.09	1.23 ± 0.00	1.23 ± 0.00	1.23 ± 0.00*
Body axial				
IQon	1.35 ± 0.11	1.39 ± 0.09*	1.44 ± 0.00*	1.44 ± 0.00*
iCT	1.27 ± 0.09	1.23 ± 0.00*	1.23 ± 0.00*	1.23 ± 0.00*
Head helical				
IQon	1.23 ± 0.00	1.23 ± 0.00	1.23 ± 0.00	1.23 ± 0.00
iCT	1.23 ± 0.00	1.23 ± 0.00	1.27 ± 0.00	1.27 ± 0.00
Head axial				
IQon	1.23 ± 0.00	1.23 ± 0.00	1.23 ± 0.00	1.23 ± 0.00
iCT	1.23 ± 0.00	1.35 ± 0.11	1.35 ± 0.11	1.27 ± 0.09

In Fig. 3, MTF curves of the 34 cm Catphan phantom, showed an increase in variation between the different tube voltages for both scanners as compared to Fig. 2. The shape and magnitude, however, were very similar compared to Fig. 2. For body scans a spatial resolution of more than 7 lp/cm was found (5% MTF). These values are comparable to the earlier results in Fig. 2.

3.A.4. Visual inspection of spatial resolution

To verify the above measurements, images of the high resolution module in the Catphan 600 phantom were visually inspected. In general, the high resolution bars are resolved slightly better on the IQon than on the iCT. In Fig. 4 some of these images are presented. These images demonstrate that the bars are clearly separable at 7 lp/cm, but start to blur at 8 lp/cm for body scans on both the IQon and the iCT. However, the bars on the IQon are somewhat more visible than on the iCT. This confirms the observation that at 5% MTF the resolution is higher than 7 lp/cm. In a similar fashion, head scans acquired on the IQon and the iCT clearly separate the bars at 6 lp/cm, but start to blur at 7 lp/cm, confirming the observation at 5% MTF.

3.A.5. Noise characterization

The noise (SD) of the different scanning protocols is shown in Table VII. For most combinations of scan types and tube voltages, the noise of the IQon was higher, but in some instances, especially for head helical scans, the noise of the iCT was higher.

In Fig. 5, the NPS curves are shown. The NPS curves of both scanners were generally similar in shape, but the curves with high tube voltage sometimes show a low frequency peak. The IQon illustrated slightly higher noise levels compared to the iCT, this difference was significant for the head helical scans at 80 kVp and scans at 120 kVp (except for head axial scans). This significant difference is mainly found in the low frequency range of the NPS (i.e., 0.16–0.64 mm^{-1}). In addition, for body helical scans at 140 kVp the tails of the NPS (i.e., >0.64 mm^{-1}) were significantly different.

For the 34 cm phantom, an increase in noise (SD) (Table VIII) is observed as compared to the 20 cm Catphan phantom (Table VII). The IQon had a significant higher

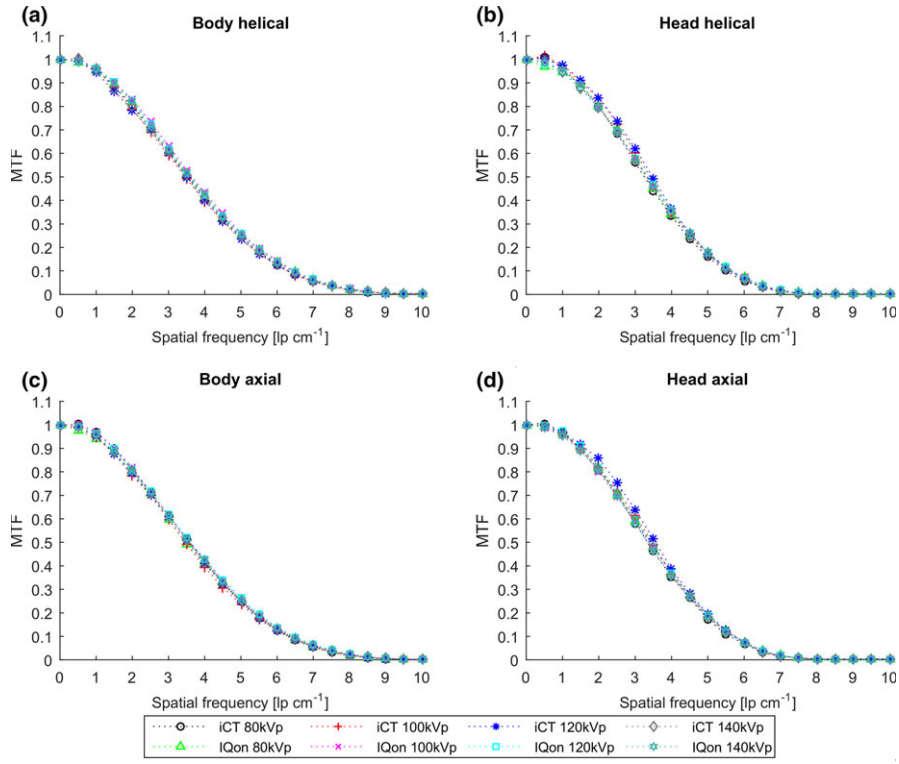

FIG. 2. Mean MTF curves of IQon and iCT for (a) body helical, (c) body axial, (b) head helical, and (d) head axial scans for all tube voltages for a phantom of 20 cm in diameter. [Color figure can be viewed at wileyonlinelibrary.com]

TABLE V. Spatial resolutions (mean ± SD) (lp/cm) at 50%, 10%, and 5% MTF, for body scans at different energies. If the difference (Diff.) between the IQon and iCT is significant, it is marked with an asterisk.

	Body helical			Body axial		
MTF	IQon	iCT	Diff.	IQon	iCT	Diff.
80 kVp						
50%	3.58 ± 0.13	3.53 ± 0.11	0.05	3.43 ± 0.17	3.57 ± 0.17	−0.14
10%	6.44 ± 0.13	6.28 ± 0.11	0.16*	6.48 ± 0.19	6.32 ± 0.17	0.17
5%	7.20 ± 0.16	7.19 ± 0.28	0.01	7.16 ± 0.17	7.09 ± 0.14	0.07
100 kVp						
50%	3.64 ± 0.16	3.45 ± 0.15	0.18*	3.60 ± 0.05	3.47 ± 0.07	0.13*
10%	6.47 ± 0.14	6.25 ± 0.10	0.22*	6.39 ± 0.07	6.26 ± 0.08	0.13*
5%	7.27 ± 0.18	7.09 ± 0.17	0.18*	7.21 ± 0.12	7.07 ± 0.10	0.15*
120 kVp						
50%	3.58 ± 0.14	3.49 ± 0.10	0.09	3.60 ± 0.09	3.54 ± 0.05	0.06
10%	6.44 ± 0.19	6.28 ± 0.11	0.16*	6.48 ± 0.07	6.32 ± 0.09	0.17*
5%	7.26 ± 0.17	7.10 ± 0.17	0.16	7.30 ± 0.14	7.19 ± 0.09	0.11*
140 kVp						
50%	3.61 ± 0.11	3.55 ± 0.06	0.07	3.57 ± 0.05	3.54 ± ± 0.05	0.02
10%	6.41 ± 0.23	6.37 ± 0.14	0.04	6.42 ± 0.07	6.36 ± 0.04	0.06*
5%	7.22 ± 0.25	7.13 ± 0.17	0.09	7.26 ± 0.11	7.22 ± 0.09	0.04

noise level as compared to the iCT for all tube voltages, except for body helical scans at 140 kVp.

In Fig. 6, the NPS curves of the 34 cm phantom are shown. These curves show that for body scans at 140 kVp there is no difference between iCT and IQon. At 80, 100, and 120 kVp, the IQon has a significant higher noise level for axial body scans. For 100 and 120 kVp, these differences are found in the tail of the NPS (i.e., >0.64 mm^{-1}), whereas at 80 kVp over the entire range of the NPS (i.e., 0.16–1.02 mm^{-1}) differences are found.

TABLE VI. Spatial resolutions (mean ± SD) (lp/cm) at 50%, 10%, and 5% MTF, for head scans at different energies. If the difference (Diff.) between the IQon and iCT is significant, it is marked with an asterisk.

	Head helical			Head axial		
MTF	IQon	iCT	Diff.	IQon	iCT	Diff.
80 kVp						
50%	3.29 ± 0.14	3.23 ± 0.19	0.06	3.42 ± 0.11	3.32 ± 0.09	0.10*
10%	5.66 ± 0.07	5.59 ± 0.10	0.07*	5.69 ± 0.08	5.74 ± 0.12	−0.05*
5%	6.26 ± 0.08	6.08 ± 0.13	0.18*	6.31 ± 0.06	6.20 ± 0.09	0.11*
100 kVp						
50%	3.32 ± 0.14	3.41 ± 0.12	−0.09	3.39 ± 0.11	3.47 ± 0.04	−0.08*
10%	5.65 ± 0.07	5.57 ± 0.10	0.08	5.72 ± 0.05	5.71 ± 0.06	0.01
5%	6.27 ± 0.08	6.17 ± 0.06	0.10*	6.32 ± 0.05	6.31 ± 0.04	0.09*
120 kVp						
50%	3.35 ± 0.09	3.47 ± 0.09	−0.13*	3.42 ± 0.06	3.55 ± 0.02	−0.14*
10%	5.66 ± 0.04	5.59 ± 0.07	0.07*	5.69 ± 0.03	5.74 ± 0.05	−0.05*
5%	6.30 ± 0.05	6.18 ± 0.04	0.12*	6.30 ± 0.04	6.31 ± 0.04	−0.01
140 kVp						
50%	3.35 ± 0.10	3.32 ± 0.05	0.03	3.35 ± 0.05	3.43 ± 0.06	−0.07*
10%	5.65 ± 0.04	5.58 ± 0.07	0.07*	5.68 ± 0.03	5.67 ± 0.03	0.01
5%	6.29 ± 0.05	6.16 ± 0.05	0.13*	6.28 ± 0.04	6.25 ± 0.03	0.03

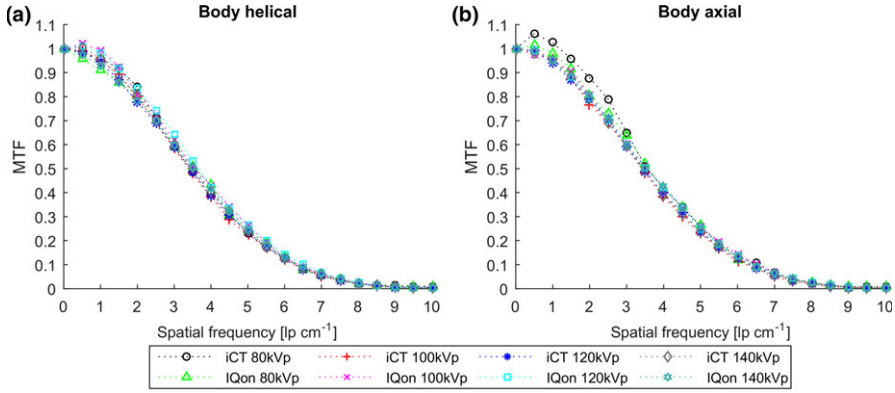

FIG. 3. Mean MTF curves of IQon and iCT for (a) body helical and (b) body axial scans for all tube voltages for a phantom of 34 cm in diameter. [Color figure can be viewed at wileyonlinelibrary.com]

In Table IX, noise levels (SD) for body scans for the 45 cm phantom are given. A significant difference is observed for all tube voltages. This difference is in favor of the iCT.

The accompanying NPS curves are shown in Fig. 7. These curves show a similar shape at all tube voltages. The differences between the iCT and IQon, were significant for all tube voltages except for body axial scans at 140 kVp. The differences in body helical scan were mainly observed in the tail of the NPS (i.e., >0.64 mm^{-1}), whereas for the body axial scans at 120 kVp over the entire range of the NPS (i.e., 0.16–1.02 mm^{-1}). In comparison to the NPS of the smaller phantoms (Figs. 5 and 6), a shift in peak frequency was observed.

3.A.6. CNR

The mean CNR of the IQon was generally slightly higher than that of the iCT, but the difference was not always significant, as can be seen in Table X. Differences up to 0.35 are seen, where the difference for head scans from IQon and iCT was significant at all tube voltages, except for head scans at 100 kVp, whereas for body scans the difference was not.

For the 34 cm phantom, the mean CNR of the IQon was generally higher than that of the iCT, as can be seen in Table XI. The differences were significant for all body helical scans, and for two of the body axial scans, including the only case where the CNR of the iCT was larger than that of the IQon (at 80 kVp). A clear decrease in CNR can be observed by comparing Table X with Table XI.

3.A.7. Mean CT values

In Table XII, the mean CT values are presented. The CT values calculated for the scans acquired at 100 kVp for the iCT, and at 120 kVp for both scanners and 140 kVp for the IQon were within the expected values of the phantom for both

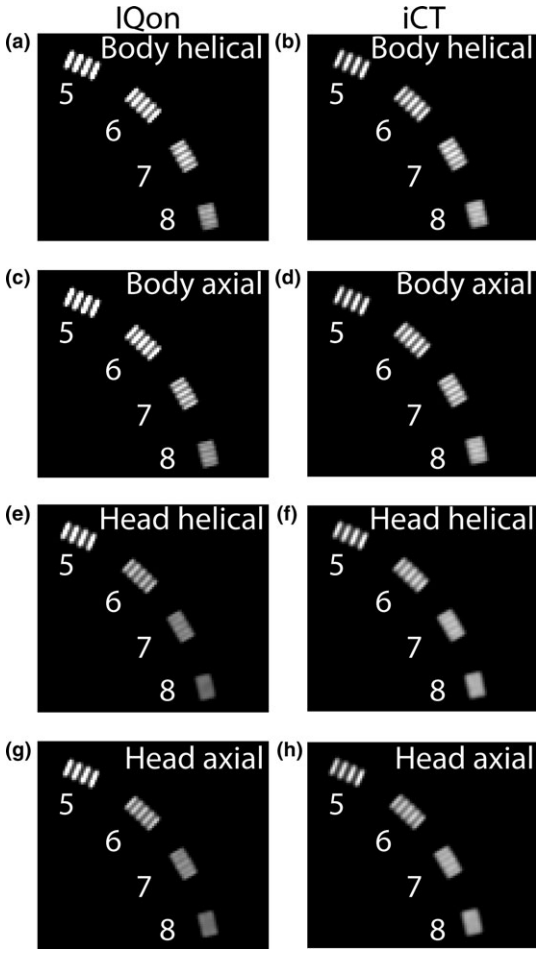

FIG. 4. High contrast resolution bars for (a,b) body helical, (c,d) body axial, (e,f) head helical, and (g,h) head axial for IQon (first column) and iCT (second column) at 140 kVp. These images are exemplary for the other tube voltages.

TABLE VII. Noise (SD) for all scan types at different energies for a phantom of 20 cm in diameter. If the difference (Diff.) (%) between IQon and iCT is significant, it is marked with an asterisk.

	80 kVp	100 kVp	120 kVp	140 kVp
Body helical				
IQon	15.31 ± 0.09	10.72 ± 0.07	8.48 ± 0.06	7.24 ± 0.11
iCT	14.83 ± 0.15	10.37 ± 0.10	8.11 ± 0.04	7.46 ± 0.08
Diff.	3.19*	3.30*	4.36*	−3.00*
Body axial				
IQon	13.44 ± 0.13	9.24 ± 0.05	7.17 ± 0.03	6.04 ± 0.05
iCT	12.72 ± 0.08	8.93 ± 0.07	6.95 ± 0.08	5.97 ± 0.02
Diff.	5.33*	3.41*	3.11*	1.32
Head helical				
IQon	11.69 ± 0.11	8.12 ± 0.03	6.32 ± 0.06	5.33 ± 0.03
iCT	12.33 ± 0.13	8.92 ± 0.07	7.38 ± 0.04	6.71 ± 0.08
Diff.	−5.46*	−9.86*	−16.80*	−25.81*
Head axial				
IQon	11.39 ± 0.08	7.88 ± 0.07	6.03 ± 0.04	5.11 ± 0.02
iCT	11.03 ± 0.10	7.65 ± 0.03	6.03 ± 0.07	5.17 ± 0.03
Diff.	3.14*	2.97*	−0.06	−1.18*

scanners. Scans acquired at 80 kVp on both scanners, scans acquired at 100 kVp on the IQon and scans acquired at 140 kVp on the iCT are not within the expected range of 5–18 HU, but are within 2% of the HU values of water (−25 to 25 HU). The difference in HU values between the iCT and the IQon is significant for all scan types at all tube voltages.

3.B. Visual impression of images

Although an observer study was beyond the scope of this study, a visual impression of the acquired images is shown in Fig. 8. The images acquired on the iCT and the IQon appear very similar with regard to noise level, contrast and resolution. The images on the iCT have a different window length, because we have to compensate for the small difference in recorded HU values between iCT and IQon. This difference in HU values was already observed in Table XII.

4. DISCUSSION

In this study, the performance of the Philips IQon Spectral CT and the Philips Brilliance iCT scanners with respect to phantom image quality of conventional images was evaluated quantitatively and qualitatively at equal dose.

A number of studies have been conducted on the dual-layer technology, primarily looking at applications of dual-energy analysis.[5,9–15] However, only few studies have yet been published on image quality of conventional images acquired on the IQon.[16,17] Ozguner et al. (2016)[16] studied the performance of DECT acquisition on the IQon by comparing image quality of mono-energetic and conventional images both acquired on the IQon. Hojjati et al. (2017)[17] evaluated conventional (diagnostic) images from the IQon and from a conventional single-layer detector scanner, both in a phantom and in abdominal clinical images to see whether the image quality and other metrics meet the requirements of ACR guidelines. But the influence of the dual-layer detector on image quality and dose of conventional images has not been established yet.

In general, the conventional images acquired on the IQon are very similar to images acquired on the iCT, as can be seen in Fig. 8. Body scans acquired on the IQon, however, demonstrated a slightly increased resolving power at each tube voltage compared with the iCT. From Table V, it can be seen that for body scans the mean MTFs at 50%, 10%, and 5% are slightly higher, albeit not always significantly. The high resolution bars confirm the above observations that for all body scans on IQon and iCT bars separated by at least 7 lp/cm are clearly visible. In the study by Hojjati et al.,[17] the resolving power for an adult body protocol was found to be 8 lp/cm for both IQon and iCT scanners. However, the authors did not mention the used settings for reconstruction kernel, FOV, and reconstruction matrix, which all influence spatial resolution. Ozguner et al.[16] demonstrated a resolving power of 7 lp/cm, also for an adult body scan, similar to the resolution found in our study. Head scans also did not always show a significant

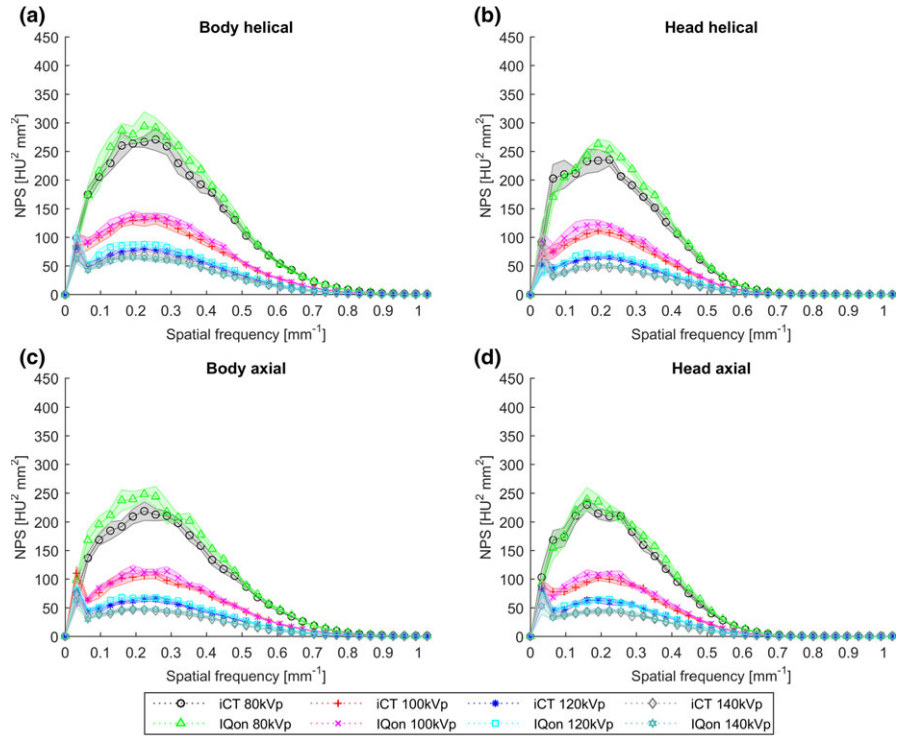

FIG. 5. Comparison of NPS curves for a phantom of 20 cm in diameter between IQon and iCT at different energies, for (a,c) body and (b,d) head scans. Mean values with 95% confidence intervals are shown. [Color figure can be viewed at wileyonlinelibrary.com]

TABLE VIII. Noise (SD) for body scans at different energies for a phantom of 34 cm in diameter. If the difference (Diff.) (%) between IQon and iCT is significant, it is marked with an asterisk.

	80 kVp	100 kVp	120 kVp	140 kVp
Body helical				
IQon	17.59 ± 0.19	12.30 ± 0.24	9.70 ± 0.12	8.13 ± 0.07
iCT	17.03 ± 0.29	11.53 ± 0.12	9.04 ± 0.16	8.17 ± 0.25
Diff.	3.17*	6.23*	6.77*	−0.51
Body axial				
IQon	15.59 ± 0.09	10.63 ± 0.07	8.28 ± 0.06	6.99 ± 0.05
iCT	14.45 ± 0.08	10.13 ± 0.07	7.89 ± 0.03	6.76 ± 0.01
Diff.	7.34*	4.73*	4.69*	3.29*

difference between the iCT and the IQon, as is confirmed visually by the high resolution bars (Fig. 4). The visual spatial resolution was found to be at least 6 lp/cm. The 34 cm phantom caused more variation in the MTF curves (Fig. 3) between the different tube voltages. However, the resolving power of body scans was similar to that of the normal 20 cm Catphan phantom, i.e., more than 7 lp/cm for both scanners.

On both scanners a shift in peak frequency was observed between the NPS measurements in the 20 and 34 cm phantoms (Figs. 5 and 6) and those in the 45 cm phantom (Fig. 7). One explanation is that the nonlinear nature of iDose[4] might start to play a role and affects spatial resolution and therefore noise texture. Another explanation might be an increase in scattering, resulting in an increase in low frequency noise.

The overall noise levels (SD) of head scans on the IQon are generally lower than those of the iCT (Table VII), and differences were significant for most tube voltages. For body scans on the other hand, the overall noise levels are generally higher on the IQon compared to the iCT (Tables VII–IX, Figs. 5–7). The differences in noise of body scans are significant for almost all tube voltages for all phantom sizes. This suggests a slightly reduced dose efficiency of the IQon for these scans compared to the iCT. This might be due to the softer beam, resulting from the reduced filtration on the IQon. Altogether, noise levels differed between both scanners, with difference in values depending on the scan situation. These noise level differences are generally significant. Yet, most observed differences are within the 15% typical variation in noise performance specified for both scanners by the vendor.[18]

An important parameter regarding image quality is CNR. CNR was studied using a 1% nominal contrast target. In general, CNR was higher for the IQon than for the iCT. The difference, however, was not always significant. The difference can be attributed mainly to the fact that on the IQon a larger contrast between the ROI and the background was observed. This larger contrast on the IQon can be attributed mainly to the difference in mean energy of the spectra of the two scanners. The attenuation of materials is energy dependent, and hence contrast is energy dependent. With decreasing mean energy, contrast increases. The reduced filtration on the IQon causes a decrease in the mean energy of the spectrum, and causes an increase in contrast as compared with the iCT. The introduction of additional attenuation, i.e., additional noise, results in a decrease in CNR (Table XI).

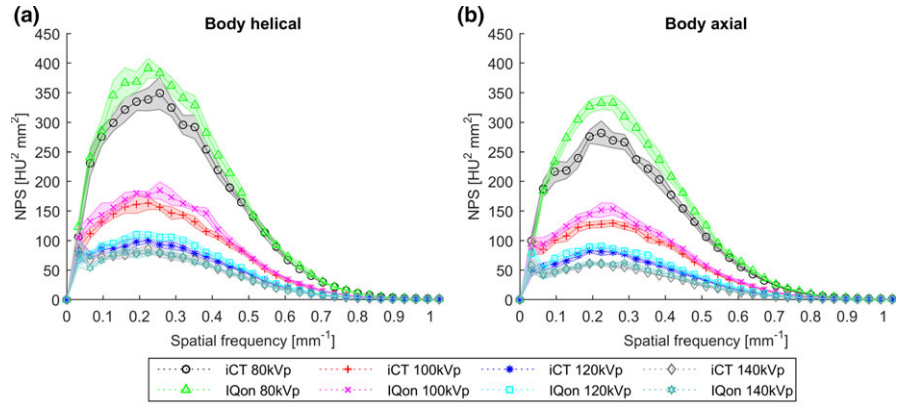

FIG. 6. Comparison of NPS curves for a phantom of 34 cm in diameter between IQon and iCT at different energies, for (a) body helical and (b) body axial scans. Mean values with 95% confidence intervals are shown. [Color figure can be viewed at wileyonlinelibrary.com]

TABLE IX. Noise (SD) for body scans at 120 and 140 kVp for a phantom of 45 cm in diameter. If the difference (Diff.) (%) between IQon and iCT is significant, it is marked with an asterisk.

	120 kVp	140 kVp
Body helical		
IQon	69.07 ± 1.34	53.84 ± 0.49
iCT	61.10 ± 0.83	53.04 ± 0.63
Diff.	11.54*	1.48*
Body axial		
IQon	57.86 ± 0.37	46.56 ± 0.18
iCT	51.08 ± 0.32	44.36 ± 0.26
Diff.	11.71*	4.74*

A reason for the difference observed in mean CT numbers between the iCT and IQon (Table XII) could be an increase in beam-hardening for the IQon compared with the iCT. The IQon has a reduced filtration, which results in an increase in low energy photons. These photons are more likely to be attenuated in the patient, which results in beam-hardening of the flux of photons. Beam-hardening is a phenomenon known for causing underestimation of CT values.[19]

This study has several limitations. First, the hybrid iterative reconstruction method iDose^4 was used. We are aware that by using this reconstruction method, image quality metrics are affected.[20–22] To illustrate these effects, we compared images reconstructed with iDose^4 (level 1) and with filtered back projection (FBP) acquired on the iCT. This comparison showed that only the magnitude of the noise and therefore the CNR was affected by the use of this reconstruction method. This was supported by the study by Löve et al.[20] The magnitude of the NPS increased by 1.23 for body scans and by 1.20 for head scans with using FBP compared to iDose^4. All other metrics were not affected by the use of iDose^4 (level 1) compared to FBP, which means that the image quality metrics used in this paper can be used sensibly with iDose^4 (level 1) reconstructed images. Secondly, the MTF and CNR should be used with care in case of nonlinear reconstruction methods such as iDose^4. Yet, for this comparative study, in which the same iterative reconstruction settings are used, these metrics improve comprehensibility and clarity. Moreover, these metrics have been widely used in multiple other comparative studies using iterative reconstruction methods.[20,23,24] Thirdly, we studied the image quality of the IQon using a fixed set of scan and reconstruction parameters, whereas other settings, for instance collimation, reconstructed slice thickness, and reconstruction kernel also have an effect on image quality.[25] Our rationale was to select the scan and reconstruction

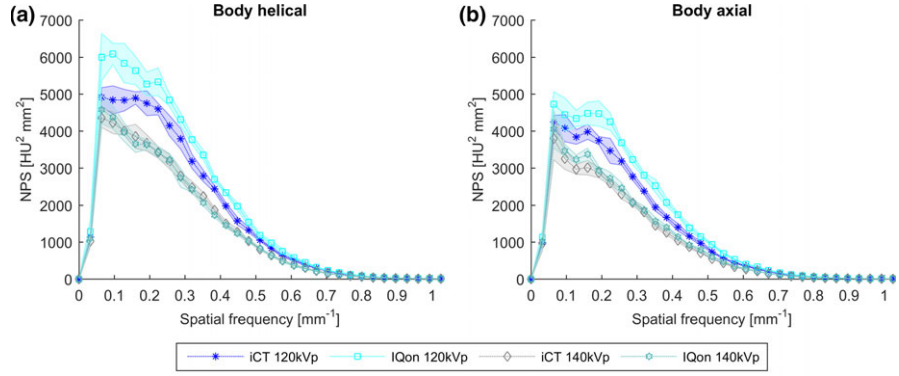

FIG. 7. Comparison of NPS curves for a phantom of 45 cm in diameter between IQon and iCT at 120 and 140 kVp, for (a) body helical and (b) body axial scans. Mean values with 95% confidence intervals are shown. [Color figure can be viewed at wileyonlinelibrary.com]

parameters that are used most at our institute and moreover are used commonly for quality control assessment.

5. CONCLUSION

The results of this work indicate that the performance of the IQon is nearly identical to the performance of the iCT in terms of CT number linearity, spatial linearity, slice thickness, and spacing for all phantom sizes. The mean CT number of the IQon was significantly different from that of the

TABLE X. CNR (mean ± SD) for all scan types at all energies. If the difference between IQon and iCT is significant, both CNR values are marked with an asterisk.

	80 kVp	100 kVp	120 kVp	140 kVp
Body helical				
IQon	0.65 ± 0.21	0.92 ± 0.18*	1.21 ± 0.21	1.51 ± 0.26
iCT	0.63 ± 0.23	1.07 ± 0.24*	1.33 ± 0.25	1.42 ± 0.28
Body axial				
IQon	0.83 ± 0.19	1.09 ± 0.19	1.54 ± 0.21*	1.76 ± 0.26*
iCT	0.77 ± 0.20	1.10 ± 0.17	1.34 ± 0.23*	1.60 ± 0.22*
Head helical				
IQon	0.92 ± 0.27*	1.35 ± 0.24	1.62 ± 0.25*	2.03 ± 0.34*
iCT	0.73 ± 0.24*	1.25 ± 0.22	1.42 ± 0.27*	1.74 ± 0.30*
Head axial				
IQon	0.91 ± 0.24*	1.33 ± 0.21	1.81 ± 0.23*	2.08 ± 0.24*
iCT	0.68 ± 0.23*	1.22 ± 0.27	1.53 ± 0.28*	1.82 ± 0.34*

TABLE XI. CNR (mean ± SD) for body scans at all energies for a phantom of 34 cm in diameter. If the difference between IQon and iCT is significant, both CNR values are marked with an asterisk.

	80 kVp	100 kVp	120 kVp	140 kVp
Body helical				
IQon	0.38 ± 0.21*	0.68 ± 0.21*	0.75 ± 0.17*	1.05 ± 0.20*
iCT	0.21 ± 0.23*	0.37 ± 0.19*	0.41 ± 0.15*	0.54 ± 0.26*
Body axial				
IQon	0.32 ± 0.16*	0.76 ± 0.18	0.94 ± 0.24	1.12 ± 0.22*
iCT	0.41 ± 0.13*	0.73 ± 0.22	0.84 ± 0.14	0.99 ± 0.20*

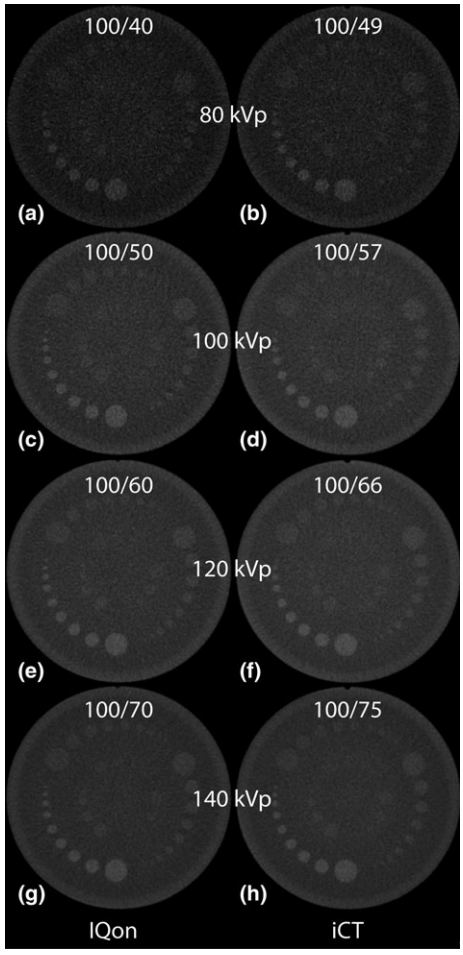

FIG. 8. Impression of images acquired at (a,b) 80 kVp, (c,d) 100 kVp, (e,f) 120 kVp, and (g,h) 140 kVp with IQon (first column) and iCT (second column); here, axial body scans are presented. The used ratio of window width and window length (W/L) is given in the images.

TABLE XII. Mean CT values (M ± SD) (HU) of uniform material, which by design has CT numbers within 2% of the HU of water (−25–25 HU), with an expected range of 5–18 HU.

	80 kVp	100 kVp	120 kVp	140 kVp
Body helical				
IQon	−19.65 ± 15.36	−0.47 ± 10.74	9.10 ± 8.48	15.69 ± 7.20
iCT	−9.07 ± 14.83	7.29 ± 10.38	15.61 ± 8.09	20.87 ± 7.48
Body axial				
IQon	−18.44 ± 13.45	0.26 ± 9.25	9.27 ± 7.18	15.52 ± 6.03
iCT	−9.36 ± 12.71	7.01 ± 8.92	15.29 ± 6.97	20.25 ± 5.97
Head helical				
IQon	−17.83 ± 11.71	−0.99 ± 8.12	8.56 ± 6.30	14.97 ± 5.34
iCT	−13.04 ± 12.26	6.54 ± 8.94	15.94 ± 7.41	20.36 ± 6.70
Head axial				
IQon	−17.15 ± 11.34	−0.56 ± 7.86	8.77 ± 6.05	14.79 ± 5.11
iCT	−10.21 ± 11.05	8.64 ± 7.67	17.69 ± 6.02	21.58 ± 5.15

iCT. While in terms of noise the iCT performed marginally better, values of contrast and resolution where slightly in favor of the IQon. Since these measures are exchangeable to some degree, we can conclude that for medium-sized (20 cm) phantoms both scanners have similar performance. For larger phantoms (34 and 45 cm) at 80–120 kVp, dose efficiency is degraded for the IQon as compared to the iCT. This suggests that the introduction of a dual-layer detector does not compromise image quality of conventional images for normal-sized patients, but slightly degrades dose efficiency for large patients at lower tube voltages.

ACKNOWLEDGMENTS

This research is supported by the Dutch heart foundation, by the Netherlands Organization for Scientific Research (NWO), domain Applied and Engineering Sciences (TTW), and by Philips Healthcare. We thank B. J. van Nierop for his theoretical support.

CONFLICTS OF INTEREST

A. Vlassenbroek is an employee of Philips Healthcare. H.W.A.M. de Jong, J.W. Dankbaar, and M.A. Viergever have received institutional support from Philips Healthcare for the current study. The other authors declare that they have no conflicts of interest to disclose.

[a)]Author to whom correspondence should be addressed. Electronic mail: f.vanommen@umcutrecht.nl; Telephone: +31 88 7567571.

REFERENCES

1. Alvarez RE, Macovski A. Energy-selective reconstructions in X-ray computerized tomography. *Phys Med Biol*. 1976;21:733–744.
2. Macovski A, Alvarez RE, Chan JLH, Stonestrom JP, Zatz LM. Energy dependent reconstruction in X-ray computerized tomography. *Comput Biol Med*. 1976;6:325–336.
3. McCollough CH, Leng S, Yu L, Fletcher JG. Dual- and multi-energy CT: principles, technical approaches, and clinical applications. *Radiology*. 2015;276:637–653.
4. Vlassenbroek A. Dual layer CT. In: Johnson T, Fink C, Schönberg SO, Reiser MF, eds. *Dual Energy CT in Clinical Practice*. Berlin, Heidelberg: Springer Berlin Heidelberg; 2011:21–34.
5. Carmi R, Kafri G, Altman A, et al. Arterial double-contrast dual-energy MDCT: in-vivo rabbit atherosclerosis with iodinated nanoparticles and gadolinium agents. 2010;(March):76261G.
6. The Phantom Laboratory Inc. Catphan 500 and 600 Manual. 2006; 1–33.
7. ICRU. Report No.87: radiation dose and image-quality assessment in computed tomography. *J ICRU*. 2012;12:9–149.
8. Nickoloff EL. Measurement of the PSF for a CT scanner: appropriate wire diameter and pixel size. *Phys Med Biol*. 1988;33:149.
9. van Hamersvelt RW, Willemink MJ, de Jong PA, et al. Feasibility and accuracy of dual-layer spectral detector computed tomography for quantification of gadolinium: a phantom study. *Eur Radiol*. 2017;27:1–10.
10. vanHamersvelt RW, Schilham AMR, Engelke K, et al. Accuracy of bone mineral density quantification using dual-layer spectral detector CT: a phantom study. *Eur Radiol*. 2017;24:1–9.
11. Neuhaus V, Abdullayev N, Große Hokamp N, et al. Improvement of image quality in unenhanced dual-layer CT of the head using virtual monoenergetic images compared with polyenergetic single-energy CT. *Invest Radiol*. 2017;27:1.
12. Oda S, Nakaura T, Utsunomiya D, et al. Clinical potential of retrospective on-demand spectral analysis using dual-layer spectral detector-computed tomography in ischemia complicating small-bowel obstruction. *Emerg Radiol*. 2017;24:7–10.
13. Wellenberg RHH, Boomsma MF, van Osch JAC, et al. Quantifying metal artefact reduction using virtual monochromatic dual-layer detector spectral CT imaging in unilateral and bilateral total hip prostheses. *Eur J Radiol*. 2017;88:61–70.
14. Hickethier T, Baeßler B, Kroeger JR, et al. Monoenergetic reconstructions for imaging of coronary artery stents using spectral detector CT: In-vitro experience and comparison to conventional images. *J Cardiovasc Comput Tomogr*. 2017;11:33–39.
15. Doerner J, Hauger M, Hickethier T, et al. Image quality evaluation of dual-layer spectral detector CT of the chest and comparison with conventional CT imaging. *Eur J Radiol*. 2017;93:52–58.
16. Ozguner O, Halliburton S, Dhanantwari A, et al. WE-FG-207B-11: objective image characterization of spectral CT with a dual-layer detector. *Med Phys*. 2016;43(6Part42):3836.
17. Hojjati M, Rassouli N, Tatsuoka C, et al. Quality of routine diagnostic images generated from a novel detector-based spectral CT scanner- A phantom and clinical study. *Abdom Radiol*. 2017;.
18. Philips. IQon spectral CT technical reference guide. 2016.
19. Zatz LM, Alvarez RE. An inaccuracy in computed tomography: the energy dependence of CT values. *Radiology*. 1977;124:91–97.
20. Löve A, Olsson M-L, Siemund R, et al. Six iterative reconstruction algorithms in brain CT: a phantom study on image quality at different radiation dose levels. *Br J Radiol*. 1031;2013:20130388.
21. Mehta D, Thompson R, Morton T, Dhanantwari A, Shefer E. Iterative model reconstruction: simultaneously lowered computed tomography radiation dose and improved image quality. *Med Phys Int*. 2013;1:86683G.
22. Willemink MJ, Takx RAP, de Jong PA, et al. Computed tomography radiation dose reduction: effect of different iterative reconstruction algorithms on image quality. *J Comput Assist Tomogr*. 2014;38:815–823.
23. Miéville FA, Gudinchet F, Brunelle F, Bochud FO, Verdun FR. Iterative reconstruction methods in two different MDCT scanners: physical metrics and 4-alternative forced-choice detectability experiments – A phantom approach. *Phys Medica*. 2013;29:99–110.
24. Harris MA, Huckle J, Anthony D, Charnock P. The acceptability of iterative reconstruction algorithms in head CT: an assessment of sinogram affirmed iterative reconstruction (SAFIRE) vs. filtered back projection (FBP) using phantoms. *J Med Imaging Radiat Sci*. 2017;48:259–269.
25. Goldman LW. Principles of CT: radiation dose and image quality. *J Nucl Med Technol*. 2007;35:213–225.